DE GRUYTER OPEN

Int. J. of Applied Mechanics and Engineering, 2017, vol.22, No.3, pp.613-636
DOI: 10.1515/ijame-2017-0039

NUMERICAL SOLUTIONS BY EFGM OF MHD CONVECTIVE FLUID FLOW PAST A VERTICAL PLATE IMMERSED IN A POROUS MEDIUM IN THE PRESENCE OF CROSS DIFFUSION EFFECTS VIA BIOT NUMBER AND CONVECTIVE BOUNDARY CONDITION

R.S. RAJU*
Department of Mathematics, GITAM University, Hyderabad Campus
Rudraram, 502329, Telangana State, INDIA
E-mail: srivass999@gmail.com

B.M. REDDY
Department of Mathematics, Bandari Srinivas Institute of Technology
Gollapally (Village), Chevella (Mandal), Ranga Reddy (District)
501503, Telangana State, INDIA

M.M. RASHIDI
Shanghai Key Lab of Vehicle Aerodynamics and Vehicle Thermal Management Systems
Tongji University
4800 Cao An Rd., Jiading, Shanghai 201804, CHINA
ENN-Tongji Clean Energy Institute of Advanced Studies
Shanghai, CHINA

R.S.R. GORLA
Department of Mechanical Engineering, University of Akron
Akron, Ohio, USA, 44325

In this investigation, the numerical results of a mixed convective MHD chemically reacting flow past a vertical plate embedded in a porous medium are presented in the presence of cross diffusion effects and convective boundary condition. Instead of the commonly used conditions of constant surface temperature or constant heat flux, a convective boundary condition is employed which makes this study unique and the results more realistic and practically useful. The momentum, energy, and concentration equations derived as coupled second-order, ordinary differential equations are solved numerically using a highly accurate and thoroughly tested element free Galerkin method (EFGM). The effects of the Soret number, Dufour number, Grashof number for heat and mass transfer, the viscous dissipation parameter, Schmidt number, chemical reaction parameter, permeability parameter and Biot number on the dimensionless velocity, temperature and concentration profiles are presented graphically. In addition, numerical results for the local skin-friction coefficient, the local Nusselt number, and the local Sherwood number are discussed through tabular forms. The discussion focuses on the physical interpretation of the results as well as their comparison with the results of previous studies.

Key words: thermal diffusion, diffusion thermo, MHD, porous medium, EFGM.

1. Introduction

The analysis of a mixed convection boundary layer flow along a vertical surface embedded in a porous medium has received considerable theoretical and practical interest. A number of studies have been

* To whom correspondence should be addressed

reported in the literature focusing on the problem of mixed convection about different surface geometries in porous media. A review of convective heat transfer in a porous medium is presented in the book by Nield and Bejan [1]. The homotopy analysis method was employed by Rashidi *et al*. [2] to free convective heat and mass transfer in a steady two-dimensional magnetohydrodynamic fluid flow over a stretching vertical surface in a porous medium. Bég *et al*. [3] investigated the combined heat and mass transfer by mixed magneto-convective flow of an electrically conducting flow along a moving radiating vertical flat plate with hydrodynamic slip and thermal convective boundary conditions. Freidoonimehr *et al*. [4] investigated the transient MHD laminar free convection flow of a nano-fluid past a vertical surface was considered porous and stretched under acceleration. The boundary-layer forms of the governing partial differential equations (momentum and energy equations) were transformed into highly nonlinear coupled ordinary differential equations (ODEs) using the fourth order Runge-Kutta method based on the shooting technique. Dinarvand *et al*. [5] found similarity solutions for the unsteady laminar incompressible boundary layer flow of a viscous electrically conducting fluid in stagnation point region of an impulsively rotating and translating sphere with a magnetic field. The buoyancy force gives a system of non-linear partial differential equations. The effect of a non-uniform magnetic field on nanofluid forced convection heat transfer in a lid driven semi-annulus was discussed by Sheikholeslami *et al*. [6]. In this paper, the authors used the control volume based finite element method to solve the governing equations in the form of stream function-vorticity formulation for the thermophoresis and Brownian motion effects. Sheikholeslami *et al*. [7] studied the forced convection heat transfer in a semi annulus lid under the influence of a variable magnetic field with the help of the control volume based finite element method. Sivaiah and Raju [8] studied the effect of Hall current on heat and mass transfer in a viscous dissipative fluid flow with a heat source using the finite element method. Garoosi *et al*. [9] carried out a numerical study concerning natural and mixed convection heat transfer of a nanofluid in a two-dimensional square cavity with numerous pairs of heat source-sinks. In this research, the authors solved two-dimensional Navier-Stokes, energy and volume fraction equations by applying the finite volume method. Makinde and Aziz [10] studied the effects of the heat and mass transfer from a vertical plate embedded in a porous medium experiencing a first-order chemical reaction and exposed to a transverse magnetic field. Anand Rao *et al*. [11] studied the effect of chemical reaction on an unsteady plate embedded in a porous medium with heat absorption. Shiva Reddy Sheri and Srinivasa Raju [12] studied the effect of viscous dissipation on a transient free convective flow past an infinite vertical porous plate in the presence of a magnetic field using the finite element method. Murthy *et al*. [13] discussed the effects of heat and mass transfer magnetohydrodynamic natural convective flow past an infinite vertical porous plate in the presence of thermal radiation and Hall current using the finite element method. Srinivasa Raju *et al*. [14] studied the application of the finite element method to unsteady MHD free convection flow past a vertically inclined porous plate including thermal diffusion and diffusion thermo effects. A mixed convection flow of electrically conducting power law fluids along a vertical wavy surface in the presence of a transverse magnetic field was studied numerically by Nejad *et al*. [15]. Xiao-dong Wang *et al*. [16] developed nonlinear mathematical models for one-dimensional flow by defining new dimensionless variables with unknown moving boundaries in semi-infinite porous media. Vajravelu *et al*. [17] studied the effects of thermo-physical properties on the flow and heat transfer in a thin film of a power-law liquid over a horizontal stretching surface in the presence of viscous dissipation. Saleem and Nadeem [18] studied the mutual effects of viscous dissipation and slip effects on a rotating vertical cone in a viscous fluid. Adesanya and Makinde [19] made the thermodynamic analysis in a forced convective flow of a third grade fluid through a vertical channel. Swati Mukhopadhyay and Vajravelu [20] investigated a two-dimensional flow of a non-Newtonian fluid over an unsteady stretching permeable surface.

When heat and mass transfer occur simultaneously in a moving fluid, the relations between the fluxes and the driving potentials are of a more integrate nature. It has been observed that an energy flux can be generated not only by temperature gradients but also by concentration gradients. The energy flux caused by a concentration gradient is termed the diffusion thermo (Dufour) effect. On the other hand, mass fluxes can also be created by temperature gradients and this embodies the thermal diffusion (Soret) effect. In most of the studies related to the heat and mass transfer process, Soret and Dufour effects are neglected on the basis that they are of a smaller order of magnitude than the effects described by Fourier and Fick laws. But

these effects are considered as second order phenomena and may become significant in areas such as hydrology, petrology, geosciences, etc. The Soret effect, for instance, has been utilized for isotope separation and in mixture between gases with very light molecular weight (H_2 or *He*) and of medium molecular weight (N_2 or *Air*). The Dufour effect was found to be of order of considerable magnitude such that it cannot be neglected ([21]). Rashidi *et al*. [22] have derived analytical expressions for the solution of steady MHD convective and slip flow due to a rotating disk by taking viscous dissipation and Ohmic heating into account. Sheri and Raju [23] studied the influence of the Soret effect on an unsteady magnetohydrodynamics free convective flow past a semi-infinite vertical plate in the presence of viscous dissipation. The results of thermal radiation and heat source on an unsteady MHD free convective fluid flow over an infinite vertical plate in the case of thermal diffusion were discussed by Raju *et al*. [24]. Rao and Raju [25] studied the effects of Hall currents, Soret and Dufour effects on the MHD flow and heat transfer along a porous flat plate with mass transfer. The results of mixed convective heat and mass transfer flow found by Srinivasacharya *et al*. [26] along a wavy surface in a Darcy porous medium were presented in the presence of cross diffusion effects. Mahdy *et al*. [27] studied laminar magnetohydrodynamic thermosolutal Marangoni convection along a vertical surface in the presence of the Soret and Dufour effects. Vedavathi *et al*. [28] dealt with the effects of heat and mass transfer on a two-dimensional unsteady MHD free convection flow past a vertical porous plate in a porous medium in the presence of thermal radiation under the influence of Dufour and Soret effects. Hsiao *et al*. [29] investigated the combined heat and mass transfer of an electrically conducting, non-Newtonian power-law fluid in MHD free convection adjacent to a vertical plate within a porous medium in the presence of the thermophoresis particle deposition effect. Pal and Chatterjee [30] studied MHD mixed convection with the combined action of Soret and Dufour effects on heat and mass transfer of a power-law fluid over an inclined plate in a porous medium in the presence of variable thermal conductivity, thermal radiation, chemical reaction and Ohmic dissipation and suction/injection. Pal and Mondal [31] dealt with the thermophoresis particle deposition and Soret-Dufour effects on the convective flow, heat and mass transfer characteristics of an incompressible Newtonian electrically conducting fluid having temperature-dependent viscosity over a non-isothermal wedge in the presence of thermal radiation. Srinivasa Raju *et al.* [32] found both analytical and numerical results of unsteady magnetohydrodynamic free convective flow past an exponentially moving vertical plate with heat absorption and chemical reaction. The free convection boundary layer flow over an arbitrarily inclined heated plate in a porous medium with Soret and Dufour effects was studied by Cheng [33] by transforming the governing equations into a universal form. Cheng [34] studied the heat and mass transfer characteristics of natural convection near a vertical wavy cone in a fluid-saturated porous medium with Soret and Dufour effects. Pal and Chatterjee [35] studied the combined Soret and Dufour effects on mixed convection magnetohydrodynamic heat and mass transfer in a micropolar fluid-saturated Darcian porous medium in the presence of thermal radiation, non-uniform heat source/sink and Ohmic dissipation. Srinivasa Raju *et al*. [36] found both analytical and numerical results of unsteady magnetohydrodynamic free convective flow past an exponentially moving vertical plate with heat absorption and chemical reaction.

Motivated by the investigations and applications mentioned above, the aim of this investigation is to consider the effects of thermal diffusion and diffusion thermo on a mixed convection flow past a vertical plate embedded in a porous medium in the presence of a chemical reaction and convective boundary condition. The governing partial differential equations are converted into ordinary differential equations by similarity transformation and are solved numerically by using the element free Galerkin method. The results obtained are presented graphically for velocity, temperature and concentration profiles for various parameters entering into the problem. The numerical values of the local skin-friction, local rate of heat and mass transfer coefficients are also presented in both graphs and tabular forms. This research paper is is an extension of the work of Makinde and Aziz [10] to include the Dufour and Soret numbers. The results obtained are in good agreement with the results of Makinde and Aziz [10] in the absence of thermal diffusion and diffusion thermo effects.

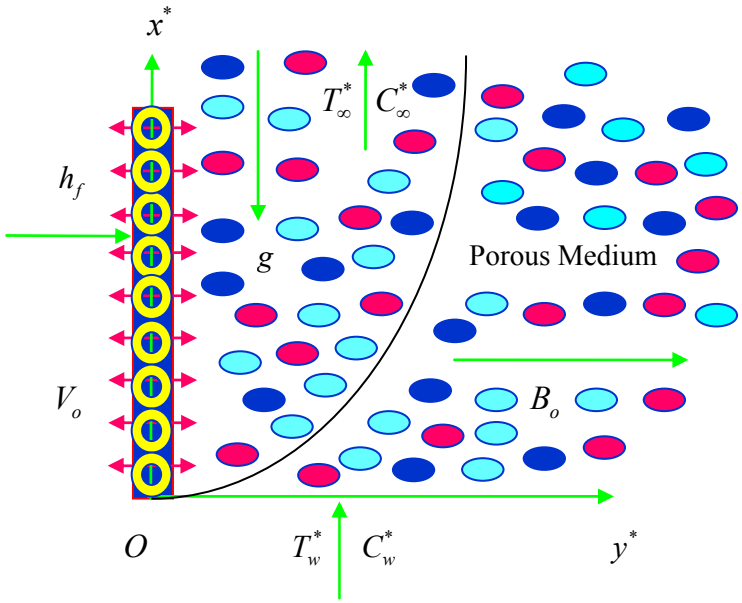

Fig.1. Physical configuration and coordinates system.

2. Mathematical formulation

The combined effects of thermal diffusion (Soret) and diffusion thermo (Dufour) on a steady, hydromagnetic mixed convection flow of a cold fluid at temperature T_∞^* over an infinite vertical plate embedded in a porous medium and subjected to a uniform transverse magnetic field and convective boundary condition is studied. The physical model and the coordinate system are shown in Fig.1. We made the following assumptions:

(i) In the Cartesian coordinate system, the x^*-axis is taken along the plate and the y^*-axis normal to the plate. Since the plate is considered infinite in the x^*-direction, hence all physical quantities will be independent of the x^*-direction.

(ii) It is assumed that the left surface of the plate is heated by convection from a hot fluid at temperature T_w^* which provides a heat transfer coefficient h_f.

(iii) The cold fluid on the right side of the plate is assumed to be Newtonian and electrically conducting.

(iv) A uniform magnetic field of magnitude B_o is applied normal to the plate. The transverse applied magnetic field and the magnetic Reynold's number are assumed to be very small for the fluid used in industrial applications, we assume that the induced magnetic field is negligible.

(v) The fluid properties are assumed to be constant except that the influence of density variation with temperature has been considered only in the body-force term.

(vi) The fluid has constant kinematic viscosity and constant thermal conductivity, and the Boussinesq approximation has been adopted for the flow.

(vii) The chemical reactions are taking place in the flow and all thermophysical properties are assumed to be constant. The linear momentum equation which is approximated according to the Boussinesq approximation.

(viii) It is assumed that there is no applied voltage which implies the absence of an electric field.

Under these assumptions, the Boussinesq and boundary layer approximations, the momentum, energy and concentration equations can be written (Makinde and Aziz [10]) as follows:

Momentum equation

$$-V_o\left(\frac{\partial u^*}{\partial y^*}\right)=\left(\nu\frac{\partial^2 u^*}{\partial y^{*2}}\right)-\left[\frac{\sigma B_o^2}{\rho}\right]u^*-\left[\frac{\nu}{K^*}\right]u^*+$$
$$+g\beta\left(T^*-T_\infty^*\right)+g\beta^{**}\left(C^*-C_\infty^*\right)+\left(\frac{\nu}{K^*}\right)U_p^*+\left(\frac{\sigma B_o^2}{\rho}\right)U_p^*. \tag{2.1}$$

Energy equation

$$-V_o\left(\frac{\partial T^*}{\partial y^*}\right)=\frac{\kappa}{\rho C_p}\left[\frac{\partial^2 T^*}{\partial y^{*2}}\right]+\frac{\nu}{C_p}\left(\frac{\partial u^*}{\partial y^*}\right)^2+\left[\frac{D_m k_T}{C_S C_p}\frac{\partial^2 C^*}{\partial y^{*2}}\right]-\left[\frac{\sigma B_o^2}{\rho C_p}\right]\left(U_p^*-u^*\right)^2. \tag{2.2}$$

Species diffusion equation

$$-V_o\left(\frac{\partial C^*}{\partial y^*}\right)=D\frac{\partial^2 C^*}{\partial y^{*2}}-K_r^*\left(C^*-C_\infty^{\prime *}\right)+\left[\frac{D_m k_T}{T_m}\frac{\partial^2 T^*}{\partial y^{*2}}\right]. \tag{2.3}$$

The term on the left hand side of Eq.(2.1) is the convective inertial (acceleration) term. On the right hand side of Eq.(2.1), the first term simulates the viscous shear effects (momentum diffusion), the second term in the square brackets represents the Lorentzian magnetohydrodynamic retarding force (acting transverse to the magnetic field), the third term in the square brackets denotes the bulk matrix resistance, i.e., Darcy term. The fourth and fifth terms on the right hand side of Eq.(2.1) are the thermal buoyancy force and species buoyancy terms. In Eq.(2.2) the term on the left hand side is the thermal convective term. On the right hand side of Eq.(2.2), the first term represents thermal diffusion, the second term represents viscous dissipative term and the third term represents species diffusion or Dufour on the temperature field. In Eq.(2.3), the term on the left hand side signifies the convective mass transfer term. On the right hand side of Eq.(2.3), the first term represents species diffusion, the second term is the chemical reaction term and the final term represents thermal diffusion or Soret.

The appropriate boundary conditions for this flow are

$$u^*=0,\quad \kappa\left(\frac{\partial T^*}{\partial y^*}\right)=h_f\left(T^*-T_w^*\right),\quad C^*=C_w^*\quad \text{at}\quad y^*=0,$$
$$u^*\to U_p^*,\quad T^*\to T_\infty^*,\quad C'\to C_\infty^*\quad \text{as}\quad y^*\to\infty \tag{2.4}$$

where the convective heating process at the plate is characterized by the hot fluid temperature T_w^* and the heat transfer coefficient h_f. Let us introduce the following dimensionless quantities

$$\eta=\frac{y^*V_o}{\nu},\ u=\frac{u^*}{V_o},\ U_p=\frac{U_p^*}{V_o},\ \theta=\frac{T^*-T_\infty^*}{T_w^*-T_\infty^*},\ \varphi=\frac{C^*-C_\infty^*}{C_w^*-C_\infty^*},\ \mathrm{Sc}=\frac{\nu}{D},\ K=\frac{K^*V_o^2}{\nu^2},$$
$$\mathrm{Gr}=\frac{g\beta\nu\left(T_w^*-T_\infty^*\right)}{V_o^3},\quad \mathrm{Gc}=\frac{g\beta^{**}\nu\left(C_w^*-C_\infty^*\right)}{V_o^3},\quad \mathrm{Pr}=\frac{\nu\rho C_p}{\kappa}, \tag{2.5}$$
$$k_r=\frac{K_r^*\nu}{V_o^2},\quad M=\left(\frac{\sigma B_o^2}{\rho}\right)\frac{\nu}{V_o^2},\quad \mathrm{Sr}=\frac{D_m k_T\left(T_w^*-T_\infty^*\right)}{\nu T_m\left(C_w^*-C_\infty^*\right)},$$
$$\mathrm{Du}=\frac{D_m k_T\left(C_w^*-C_\infty^*\right)}{\nu C_S C_p\left(T_w^*-T_\infty^*\right)},\quad \mathrm{Ec}=\frac{V_o^2}{C_p\left(T_w^*-T_\infty^*\right)},\quad \mathrm{Bn}=\frac{h_f\nu}{\kappa V_o},\quad \mathrm{Re}_x=-\frac{V_o x}{\nu}\cdot$$

In view of Eq.(2.5), Eqs (2.1) to (2.3) may be written in a dimensionless form as follows:
Momentum equation

$$u'' + u' + (\mathrm{Gr})\theta + (\mathrm{Gc})\varphi + M\left(U_p - u\right) + \frac{\left(U_p - u\right)}{K} = 0 \tag{2.6}$$

Energy equation

$$\theta'' + (\mathrm{Pr})\theta' + (M)(\mathrm{Ec})(\mathrm{Pr})\left(U_p - u\right)^2 + (\mathrm{Ec})(\mathrm{Pr})(u')^2 + (\mathrm{Du})(\mathrm{Pr})(\varphi'') = 0 \tag{2.7}$$

Concentration equation

$$\varphi'' + (\mathrm{Sc})\varphi' - (k_r)(\mathrm{Sc})\varphi + (\mathrm{Sr})(\mathrm{Sc})(\theta'') = 0 \tag{2.8}$$

The corresponding initial and boundary conditions in a dimensionless form are

$$\begin{aligned} &u = 0, \quad \theta' = \mathrm{Bn}(\theta - 1), \quad \varphi = 1 \quad \text{at} \quad \eta = 0, \\ &u \to U_p, \quad \theta \to 0, \quad \varphi \to 0 \quad \text{as} \quad \eta \to \infty \end{aligned} \tag{2.9}$$

All the physical parameters are defined in the nomenclature. It is now important to calculate the physical quantities of primary interest, which are the local wall shear stress, the local surface heat and mass flux.

Skin-friction: Knowing the velocity field, the skin-friction at the plate can be obtained, which in a non-dimensional form is given by

$$C_f = \frac{\tau_w^*}{\rho V_o^2} = \left[\frac{\partial u}{\partial \eta}\right]_{\eta=0} = u'(0). \tag{2.10}$$

Nusselt number: Knowing the temperature field, the heat transfer coefficient can be obtained, which in a non-dimensional form, in terms of the Nusselt number, is given by

$$\mathrm{Nu} = -\left[\frac{x^*}{\left(T_w^* - T_\infty^*\right)}\frac{\partial T^*}{\partial y^*}\right]_{y^*=0} \Rightarrow \mathrm{Nu}\left(\mathrm{Re}_x^{-1}\right) = -\left[\frac{\partial \theta}{\partial \eta}\right]_{\eta=0} = -\theta'(0). \tag{2.11}$$

Sherwood number: Knowing the concentration filed, the rate of mass transfer coefficient can be obtained, which in a non-dimensional form, in terms of the Sherwood number, is given by

$$\mathrm{Sh} = -\left[\frac{x^*}{\left(C_w^* - C_\infty^*\right)}\frac{\partial C^*}{\partial y^*}\right]_{y^*=0} \Rightarrow \mathrm{Sh}\left(\mathrm{Re}_x^{-1}\right) = -\left[\frac{\partial \varphi}{\partial \eta}\right]_{\eta=0} = -\varphi'(0). \tag{2.12}$$

3. Numerical solution by EFGM, study of grid independence and comparison with previous research work

3.1. Review of the Element Free Galerkin Method

The Element Free Galerkin Method (EFGM) requires moving least square (MLS) interpolation functions to approximate an unknown function, which is made up of three components: a weight function associated with each node, a basis function and a set of coefficients that depends on position. The weight function is non-zero over a small neighborhood at a particular node, called support of the node. Using the MLS approximation, the unknown velocity component u is approximated over the domain $[0, \infty]$ as

$$u(x) \cong u^h(x) = \sum_{j=1}^{m} p_j(x) a_j(x) = p^T(x) a(x) \tag{3.1}$$

where m is the number of terms in the basis, $p_j(x)$ the monomial basis function, $a_j(x)$ the non-constant coefficients and $p^T(x) = [x]$. The coefficients $a_j(x)$ are determined by minimizing the functional $J(x)$ given by

$$J(x) = \sum_{i=1}^{m} w(x - x_i) \left\{ \sum_{j=1}^{m} p_j(x_i) a_j(x) - u_i \right\}^2 \tag{3.2}$$

where $w(x - x_i)$ is a weight function which is non-zero over a small domain, called domain of influence, n is the number of nodes in the domain of influence. The minimization of $J(x)$ with respect to $a(x)$ leads to the following set of equations

$$a(x) = C^{-1}(x) D(x) U^T \tag{3.3}$$

where C and D are given as

$$C = \sum_{i=1}^{n} w(x - x_i) p(x_i) p^T(x_i), \tag{3.4}$$

$$D(x) = \left[w(x - x_1) p(x_1), w(x - x_2) p(x_2), w(x - x_3) p(x_3), ..., w(x - x_n) p(x_n) \right], \tag{3.5}$$

$$U^T = [U_1, U_2, U_3, ..., U_n]. \tag{3.6}$$

Substituting Eq.(3.3) in Eq.(3.1), the MLS approximants are obtained as

$$u(x) \cong u^h(x) = \sum_{i=1}^{n} \Phi_i(x) u_i = \Phi(x) u . \tag{3.7}$$

Similarly, $\theta(x)$, $\varphi(x)$ can be approximated by

$$\theta(x) \cong \theta^h(x) = \sum_{i=1}^{n} \Phi_i(x)\theta_i = \Phi(x)\theta, \tag{3.8}$$

$$\varphi(x) \cong \varphi^h(x) = \sum_{i=1}^{n} \Phi_i(x)\varphi_i = \Phi(x)\varphi \tag{3.9}$$

where the shape function $\Phi_i(x)$ is defined by

$$\Phi_i(x) = \sum_{j=1}^{n} p_j(x)\left(C^{-1}(x)D(x)\right)_{ji} = p^T C^{-1} D_i \ . \tag{3.10}$$

3.2. Choice of weight function

The weight function is non-zero over a small neighborhood of x_i, called the domain of the influence of node i. The choice of weight function $w(x-x_i)$ affects the resulting approximation in the EFG and other meshless methods. Singh *et al.* [37] studied these weight functions and found that a cubicspline weight function gives more accurate results as compared to others. Therefore, in the present work, the cubicspline weight function (Singh *et al*. [37]) is used.

Cubicspline weight function

$$w(r-r_i) = w(r) = \begin{Bmatrix} \frac{2}{3} - 4r^2 + 4r^3 & \text{for} & r \le \frac{1}{2} \\ \frac{4}{3} - 4r + 4r^2 - \frac{4}{3}r^3 & \text{for} & \frac{1}{2} \le r \le 1 \\ 0 & \text{for} & r > 1 \end{Bmatrix} \tag{3.11}$$

where $r_i = \dfrac{\|x - x_i\|}{d_{ml}}$, d_{ml} are the sizes of domain of influence which are calculated as $d_{ml} = d_{\max} C_i$, where $d_{\max}$ is a scaling parameter, and C_i is the distance to the nearest neighbors. The size of the domain of influence (d_{ml}) at particular node i is only controlled by the scaling parameter $(d_{\max})$ since the distance between nearest neighbors for an evaluation point remains unchanged for a given nodal data distribution. The minimum value of $d_{\max}$ should be greater than 1 so that $n > m$, and the maximum value of $d_{\max}$ should be such that it preserves the local character of the MLS approximation. It has been shown in Singh [38] that $1 < d_{\max} < 1.5$ is the optimum range of scaling parameter for heat transfer problem. Therefore $d_{\max}$ has been fixed as *1.01*. The weighted integral forms of Eqs (2.6)-(2.8) can be written as

$$\int_0^{\eta_{\max}} w_1 \left[\frac{\partial^2 u}{\partial \eta^2} + \left(\frac{\partial u}{\partial \eta} \right) - \mathrm{Nu} + NU_p + \mathrm{Gr}\theta + \mathrm{Gc}\varphi \right] d\eta = 0, \tag{3.12}$$

$$\begin{aligned} &\int_0^{\eta_{\max}} w_2 \left[\frac{\partial^2 \theta}{\partial \eta^2} + (\mathrm{Pr})\left(\frac{\partial \theta}{\partial \eta} \right) + (\mathrm{Ec})(\mathrm{Pr})\left(\frac{\partial u}{\partial \eta} \right)^2 + (M)(\mathrm{Pr})(\mathrm{Ec})(U_p - u)^2 + \right. \\ &\left. + (\mathrm{Du})(\mathrm{Pr})\left(\frac{\partial^2 \varphi}{\partial \eta^2} \right) \right] d\eta = 0, \end{aligned} \tag{3.13}$$

$$\int_0^{\eta_{\max}} w_3\left[\frac{\partial^2\varphi}{\partial\eta^2}+(\mathrm{Sc})\left(\frac{\partial\varphi}{\partial\eta}\right)-(k_r)(\mathrm{Sc})\varphi+(\mathrm{Sc})(\mathrm{Sr})\left(\frac{\partial^2\theta}{\partial\eta^2}\right)\right]d\eta=0 \tag{3.14}$$

where $N=M+\frac{1}{K}$ and w_1, w_2, w_3 are arbitrary test functions and may be viewed as the variation in u, θ and φ, respectively. After reducing the order of integration and non-linearity, we arrive at the following system of equations

$$\int_0^{\eta_{\max}}\left[\left(\frac{\partial u}{\partial\eta}\right)+\left(\frac{\partial w_1}{\partial\eta}\right)\left(\frac{\partial u}{\partial\eta}\right)-N(w_1)u+N(w_1)U_p+(\mathrm{Gr})(w_1)\theta+(\mathrm{Gc})(w_1)\varphi\right]dy+$$
$$-\left[(w_1)\left(\frac{\partial u}{\partial\eta}\right)\right]_0^{\eta_{\max}}=0, \tag{3.15}$$

$$\int_0^{\eta_{\max}}\left[(\mathrm{Pr})(w_2)\left(\frac{\partial\theta}{\partial\eta}\right)+\left(\frac{\partial w_2}{\partial\eta}\right)\left(\frac{\partial\theta}{\partial\eta}\right)+(M)(\mathrm{Pr})(\mathrm{Ec})(w_2)\left(U_p-u\right)^2+\right.$$
$$\left.+(\mathrm{Ec})(\mathrm{Pr})(w_2)\left(\frac{\partial\bar{u}}{\partial y}\right)\left(\frac{\partial u}{\partial y}\right)+(\mathrm{Du})(\mathrm{Pr})(w_2)\left(\frac{\partial w_2}{\partial\eta}\right)\left(\frac{\partial\varphi}{\partial\eta}\right)\right]d\eta+ \tag{3.16}$$
$$-\left[(w_2)\left(\frac{\partial\theta}{\partial\eta}\right)+(\mathrm{Du})(w_2)\left(\frac{\partial\varphi}{\partial\eta}\right)\right]_0^{\eta_{\max}}=0,$$

$$\int_0^{\eta_{\max}}\left[(\mathrm{Sc})(w_3)\left(\frac{\partial\varphi}{\partial\eta}\right)+\left(\frac{\partial w_3}{\partial\eta}\right)\left(\frac{\partial\varphi}{\partial\eta}\right)-(k_r)(\mathrm{Sc})(w_3)\varphi+\right.$$
$$\left.+(\mathrm{Sc})(\mathrm{Sr})(w_3)\left(\frac{\partial w_3}{\partial\eta}\right)\left(\frac{\partial\theta}{\partial\eta}\right)\right]d\eta-\left[(w_3)\left(\frac{\partial\varphi}{\partial\eta}\right)+(\mathrm{Sr})(w_3)\left(\frac{\partial\theta}{\partial\eta}\right)\right]_0^{\eta_{\max}}=0. \tag{3.17}$$

Using the essential boundary condition on w_1, w_2, w_3 as homogeneous, Eqs (3.15)-(3.17) become

$$\int_0^{\eta_{\max}}\left[\left(\frac{\partial u}{\partial\eta}\right)+\left(\frac{\partial w_1}{\partial\eta}\right)\left(\frac{\partial u}{\partial\eta}\right)-N(w_1)u+N(w_1)U_p+(\mathrm{Gr})(w_1)\theta+(\mathrm{Gc})(w_1)\varphi\right]dy=0\ , \tag{3.18}$$

$$\int_0^{\eta_{\max}}\left[(\mathrm{Pr})(w_2)\left(\frac{\partial\theta}{\partial\eta}\right)+\left(\frac{\partial w_2}{\partial\eta}\right)\left(\frac{\partial\theta}{\partial\eta}\right)+(M)(\mathrm{Pr})(\mathrm{Ec})(w_2)\left(U_p-u\right)^2+\right.$$
$$\left.+(\mathrm{Ec})(\mathrm{Pr})(w_2)\left(\frac{\partial\bar{u}}{\partial y}\right)\left(\frac{\partial u}{\partial y}\right)+(\mathrm{Du})(\mathrm{Pr})(w_2)\left(\frac{\partial w_2}{\partial\eta}\right)\left(\frac{\partial\varphi}{\partial\eta}\right)\right]d\eta=0, \tag{3.19}$$

$$\int_0^{\eta_{\max}}\left[(\mathrm{Sc})(w_3)\left(\frac{\partial\varphi}{\partial\eta}\right)+\left(\frac{\partial w_3}{\partial\eta}\right)\left(\frac{\partial\varphi}{\partial\eta}\right)-(k_r)(\mathrm{Sc})(w_3)\varphi+\right.$$
$$\left.+(\mathrm{Sc})(\mathrm{Sr})(w_3)\left(\frac{\partial w_3}{\partial\eta}\right)\left(\frac{\partial\theta}{\partial\eta}\right)\right]d\eta=0. \tag{3.20}$$

3.3. Essential boundary conditions

Due to the lack of Kronecker delta property in the EFG, the shape function Φ_i has some difficulty in the imposition of essential boundary conditions. To remove this problem, different numerical techniques have been proposed to enforce the essential boundary condition in the EFG method such as the Lagrange multiplier technique, modified variational principle approach and penalty approach. The penalty method (Zhu and Atluri [39]) is applied:

Penalty Method (PM)

$$\int_0^{\eta_{max}} \left[(w_1)\left(\frac{\partial u}{\partial \eta}\right) + \left(\frac{\partial w_1}{\partial \eta}\right)\left(\frac{\partial u}{\partial \eta}\right) - N(w_1)u + N(w_1)U_p + \right.$$
$$\left. + (\mathrm{Gr})(w_1)\theta + (\mathrm{Gc})(w_1)\varphi \right] d\eta + \alpha(w_1)(u - u_o)\big|_{\eta=0} + \tag{3.21}$$
$$+ \alpha(w_1)(u - u_\infty)\big|_{\eta\to\infty} = 0,$$

$$\int_0^{\eta_{max}} \left[(\mathrm{Pr})(w_2)\left(\frac{\partial \theta}{\partial \eta}\right) + \left(\frac{\partial w_2}{\partial \eta}\right)\left(\frac{\partial \theta}{\partial \eta}\right) + (M)(\mathrm{Pr})(\mathrm{Ec})(w_2)(U_p - u)^2 + \right.$$
$$\left. + (\mathrm{Ec})(\mathrm{Pr})(w_2)\left(\frac{\partial \bar{u}}{\partial \eta}\right)\left(\frac{\partial u}{\partial \eta}\right) + (\mathrm{Du})(\mathrm{Pr})(w_2)\left(\frac{\partial w_2}{\partial \eta}\right)\left(\frac{\partial \varphi}{\partial \eta}\right) \right] d\eta + \tag{3.22}$$
$$+ \alpha(w_2)(\theta - \theta_o)\big|_{\eta=0} + \alpha(w_2)(\theta - \theta_\infty)\big|_{\eta\to\infty} = 0,$$

$$\int_0^{\eta_{max}} \left[(\mathrm{Sc})(w_3)\left(\frac{\partial \varphi}{\partial \eta}\right) + \left(\frac{\partial w_3}{\partial \eta}\right)\left(\frac{\partial \varphi}{\partial \eta}\right) - (k_r)(\mathrm{Sc})(w_3)\varphi + \right.$$
$$\left. + (\mathrm{Sc})(\mathrm{Sr})(w_3)\left(\frac{\partial w_3}{\partial \eta}\right)\left(\frac{\partial \theta}{\partial \eta}\right) \right] d\eta + \alpha(w_3)(\varphi - \varphi_o)\big|_{\eta=0} + \tag{3.23}$$
$$+ \alpha(w_3)(\varphi - \varphi_\infty)\big|_{\eta\to\infty} = 0$$

where $u_o = 0,\ \theta_o = \mathrm{Bn}(\theta - 1),\ \varphi_o = 1,\ u_\infty = U_p,\ \theta_\infty = 0,\ \varphi_\infty = 0$ and $w_1 = w_2 = w_3 = \Phi_i\ (i = 1, 2, \ldots\ldots n)$

Thus Eqs (3.21)-(3.23) can be written as

$$[K]\{\bar{h}\} + [\bar{M}]\{\dot{\bar{h}}\} = \{F\} \tag{3.24}$$

where $[K] = \begin{bmatrix} K_{11} & K_{12} & K_{13} \\ K_{21} & K_{22} & K_{23} \\ K_{31} & K_{32} & K_{33} \end{bmatrix},\ [\bar{M}] = \begin{bmatrix} Moo \\ oMo \\ ooM \end{bmatrix},\ \{\bar{h}\} = \begin{bmatrix} \{u\} \\ \{\theta\} \\ \{\varphi\} \end{bmatrix},\ \{\dot{\bar{h}}\} = \begin{bmatrix} \{\dot{u}\} \\ \{\dot{\theta}\} \\ \{\dot{\varphi}\} \end{bmatrix},\ \{F\} = \begin{bmatrix} \{F_1\} \\ \{F_2\} \\ \{F_3\} \end{bmatrix},$

$$(K_{11})_{ij} = -\int_0^{\eta_{max}} \left[\left(\Phi_i^T\right)\left(\Phi'_j\right) \right] d\eta - \int_0^{\eta_{max}} \left[\left(\Phi_i^{T'}\right)\left(\Phi'_j\right) \right] d\eta - N \int_0^{\eta_{max}} \left[\left(\Phi_i^T\right)\left(\Phi_j\right) \right] d\eta +$$
$$-N(U_p) \int_0^{\eta_{max}} \left[\Phi_i^T \right] d\eta + \left[\alpha\left(\Phi_i^T\right)\left(\Phi_j\right) \right]_{\eta=0} \left[\alpha\left(\Phi_i^T\right)\left(\Phi_j\right) \right]_{\eta\to\infty},$$

$$(K_{12})_{ij} = -(\mathrm{Gr}) \int_0^{\eta_{\max}} \left(\Phi_i^T\right)\left(\Phi_j\right) d\eta, \qquad (K_{13})_{ij} = -(\mathrm{Gc}) \int_0^{\eta_{\max}} \left(\Phi_i^T\right)\left(\Phi_j\right) d\eta,$$

$$(M)_{ij} = \int_0^{\eta_{\max}} \left(\Phi_i^T\right)\left(\Phi_j\right) d\eta, \qquad (F_1)_i = u_o \alpha \Phi'_j + u_\infty \alpha \Phi'_j,$$

$$(K_{21})_{ij} = -(\mathrm{Ec})(\mathrm{Pr}) \int_0^{\eta_{\max}} \left[\left(\Phi_i^T\right)\left(\frac{\partial \bar{u}}{\partial \eta}\right)\left(\Phi'_j\right)\right] d\eta - (\mathrm{Du})(\mathrm{Pr}) \int_0^{\eta_{\max}} \left[\left(\Phi_i^{T'}\right)\left(\Phi'_j\right)\right] d\eta,$$

$$(F_2)_i = \theta_o \alpha \Phi'_j + \theta_\infty \alpha \Phi'_j, \qquad (F_3)_i = \varphi_o \alpha \Phi'_j + \varphi_\infty \alpha \Phi'_j,$$

$$(K_{22})_{ij} = -(\mathrm{Pr}) \int_0^{\eta_{\max}} \left[\left(\Phi_i^T\right)\left(\Phi'_j\right)\right] d\eta - \int_0^{\eta_{\max}} \left[\left(\Phi_i^{T'}\right)\left(\Phi'_j\right)\right] d\eta +$$
$$+ \left[\alpha\left(\Phi_i^T\right)\left(\Phi_j\right)\right]_{\eta=0} \left[\alpha\left(\Phi_i^T\right)\left(\Phi_j\right)\right]_{\eta\to\infty},$$

$$(K_{23})_{ij} = -(M)(\mathrm{Ec})(\mathrm{Pr}) \int_0^{\eta_{\max}} \left[\left(\Phi_i^T\right)\left(U_p - u\right)^2\right] d\eta, \qquad (K_{31})_{ij} = 0,$$

$$(K_{33})_{ij} = -(\mathrm{Sc}) \int_0^{\eta_{\max}} \left[\left(\Phi_i^T\right)\left(\Phi'_j\right)\right] d\eta - \int_0^{\eta_{\max}} \left[\left(\Phi_i^{T'}\right)\left(\Phi'_j\right)\right] d\eta +$$
$$+ \left[\alpha\left(\Phi_i^T\right)\left(\Phi_j\right)\right]_{\eta=0} \left[\alpha\left(\Phi_i^T\right)\left(\Phi_j\right)\right]_{\eta\to\infty},$$

$$(K_{32})_{ij} = (\mathrm{Sc})(k_r) \int_0^{\eta_{\max}} \left[\left(\Phi_i^T\right)\left(\Phi_j\right)\right] d\eta - (\mathrm{Sc})(\mathrm{Sr}) \int_0^{\eta_{\max}} \left[\left(\Phi_i^{T'}\right)\left(\Phi'_j\right)\right] d\eta.$$

Using the unconditionally stable Crank-Nicholson scheme (Smith [40]), Eq.(3.24) at $(s+1)^{th}$ level can be written as

$$\left[\hat{K}\right]_{s+1} \left\{\bar{h}\right\}_{s+1} = \left[\hat{K}\right]_s \left\{\bar{h}\right\}_s + \left\{\hat{F}\right\}_{s,\, s+1} \tag{3.25}$$

where $$\left[\hat{K}\right]_{s+1} = \left[\bar{M}\right] + \frac{\Delta t \left[K\right]_{s+1}}{2}, \quad \left[\hat{K}\right]_s = \left[\bar{M}\right] - \frac{\Delta t \left[K\right]_s}{2}, \quad \left[\hat{F}\right]_{s,\, s+1} = \frac{\Delta t}{2}\left(\left\{F\right\}_{s+1} + \left\{F\right\}_s\right)\Bigg\}. \tag{3.26}$$

For computational purposes, the coordinate η is varied from *0* to $\eta_{\max} = 90$, where $\eta_{\max}$ represents infinity, i.e., external to the momentum, energy and concentration boundary layers. The whole domain is divided into 301 nodes. One-point Gauss quadrature formula has been used to calculate the integral values. As the systems of equations are non-linear, therefore an iterative scheme is employed to solve the matrix

system. This system is linearized by incorporating a known function u, which is solved using the Gauss elimination method maintaining an accuracy of 0.000005 . The code of the algorithm has been executed in MATLAB running on a PC. An excellent convergence was achieved for all the results.

Table 1. The numerical values of u, θ and ϕ for variation of mesh sizes.

	Mesh (Grid) Size = *0.01*			Mesh (Grid) Size = *0.001*			Mesh (Grid) Size = *0.0001*		
	u	θ	ϕ	u	θ	ϕ	u	θ	ϕ
Bn=1.0	*0.0000000000*	*0.3000000119*	*1.0000000000*	*0.0000000000*	*0.3000000119*	*1.0000000000*	*0.0000000000*	*0.3000000119*	*1.0000000000*
	1.7971072197	*0.2005633265*	*0.2327537686*	*1.7971072197*	*0.2005633265*	*0.2327537686*	*1.7971072197*	*0.2005633265*	*0.2327537686*
	1.1730452776	*0.0868006274*	*0.0628763288*	*1.1730452776*	*0.0868006274*	*0.0628763288*	*1.1730452776*	*0.0868006274*	*0.0628763288*
	0.7699034214	*0.0334579609*	*0.0191567093*	*0.7699034214*	*0.0334579609*	*0.0191567093*	*0.7699034214*	*0.0334579609*	*0.0191567093*
	0.6004918814	*0.0123445718*	*0.0063032545*	*0.6004918814*	*0.0123445718*	*0.0063032545*	*0.6004918814*	*0.0123445718*	*0.0063032545*
	0.5364440084	*0.0044701407*	*0.0021628896*	*0.5364440084*	*0.0044701407*	*0.0021628896*	*0.5364440084*	*0.0044701407*	*0.0021628896*
	0.5130777359	*0.0016032076*	*0.0007577343*	*0.5130777359*	*0.0016032076*	*0.0007577343*	*0.5130777359*	*0.0016032076*	*0.0007577343*
	0.5046514273	*0.0005688940*	*0.0002678586*	*0.5046514273*	*0.0005688940*	*0.0002678586*	*0.5046514273*	*0.0005688940*	*0.0002678586*
	0.5016060472	*0.0001949616*	*0.0000945298*	*0.5016060472*	*0.0001949616*	*0.0000945298*	*0.5016060472*	*0.0001949616*	*0.0000945298*
	0.5004715919	*0.0000561448*	*0.0000313491*	*0.5004715919*	*0.0000561448*	*0.0000313491*	*0.5004715919*	*0.0000561448*	*0.0000313491*
	0.5000000000	*0.0000000000*	*0.0000000000*	*0.5000000000*	*0.0000000000*	*0.0000000000*	*0.5000000000*	*0.0000000000*	*0.0000000000*

Study of Grid Independence: In general, to study the grid independency/dependency, we should know the mesh size should be varied in order to check the solution at different mesh (grid) sizes and get a range at which there is no variation in the solution. We showed the numerical values of velocity (u), temperature (θ) and concentration (ϕ) for different values of mesh (grid) size for different values of $Bn = 1.0$ in Tab.1. From this table, we observed that there is no variation in the values of velocity (u), temperature (θ) and concentration (ϕ) for different values of the mesh (grid) size for $Bn = 1.0$. Hence, we conclude that the results are independent of the mesh (grid) size.

Comparison with previous research work: The present results (under some limiting conditions) are compared with those of Makinde and Aziz [10] in Tab.2. An excellent agreement has been found with their results, which confirms that the present numerical solutions of the problem are correct and computed values are accurate.

Table 2. Numerical values of $u'(0)$, $-\theta'(0)$ and $-\varphi'(0)$ with Gr = *0.1*, Gc = *0.1*, Pr = *0.71*, Sc = *0.24* and $U_p = 0.5$.

							Present Element free Galerkin method results			Sixth order Runge-Kutta Method results of Makinde and Aziz [10]		
M	K	kr	Bn	Ec	Sr	Du	$u'(0)$	$-\theta'(0)$	$-\phi'(0)$	$u'(0)^{\Theta}$	$-\theta'(0)^{\Theta}$	$-\phi'(0)^{\Theta}$
0.1	*0.1*	*0.1*	*0.0*	*0.1*	*0.0*	*0.0*	*1.891555124*	*0.000000000*	*0.459012311*	*1.891555*	*0.000000*	*0.459012*
1.0							*1.962039306*	*0.083172669*	*0.459012311*	*1.862039*	*0.083172*	*0.459012*
10.0							*2.526743816*	*0.080068552*	*0.459012311*	*1.826743*	*0.080068*	*0.459012*
	1.0						*0.930812197*	*0.085574432*	*0.459012311*	*0.930812*	*0.085574*	*0.459012*
	10.0						*0.759132115*	*0.085543169*	*0.459012311*	*0.759132*	*0.085543*	*0.459012*
		1.0					*1.889451607*	*0.083620068*	*1.127174099*	*1.889451*	*0.083620*	*1.127174*
		2.0					*1.886928855*	*0.083615016*	*1.539295169*	*1.886928*	*0.083615*	*1.539295*
			1.0				*1.907655691*	*0.398302309*	*0.459012385*	*1.907655*	*0.398302*	*0.459012*
			10.0				*1.917383305*	*0.638954197*	*0.459012385*	*1.917383*	*0.638954*	*0.459012*
				1.0			*1.907091911*	*0.044871116*	*0.459012385*	*1.907091*	*0.044871*	*0.459012*
				2.0			*1.920915361*	*0.050865522*	*0.459012385*	*1.920915*	*0.050865*	*0.459012*
					1.0		*1.991065421*	*0.000532168*	*0.472281578*	*0.000000*	*0.000000*	*0.000000*
					2.0		*2.133526941*	*0.000638197*	*0.492276054*	*0.000000*	*0.000000*	*0.000000*
						1.0	*2.061588512*	*0.153916278*	*0.459206478*	*0.000000*	*0.000000*	*0.000000*
						2.0	*2.140619924*	*0.210945624*	*0.460921378*	*0.000000*	*0.000000*	*0.000000*

4. Results and discussion

In the previous sections, we have formulated and solved the problem of the influence of thermal diffusion (Soret effects) and diffusion thermo (Dufour effects) on a magnetohydrodynamic mixed convective flow past a vertical plate embedded in a porous medium with chemical reaction and convective boundary condition. Final results are computed for a variety of physical parameters which are presented by means of graphs and tabular forms. The results are obtained to illustrate the influence of the Soret number, Dufour number, Grashof number for heat and mass transfer, the viscous dissipation parameter, Schmidt number, chemical reaction parameter, permeability parameter and Biot number on the velocity, temperature and the concentration profiles, while the values of some of the physical parameters are taken as constant such as Pr = *0.71* which correspond to air and $U_p = 0.5$ in all the tables and figures. In addition, the boundary condition $\eta \to \infty$ is approximated by $\eta_{max} = 90$, which is sufficiently large for the velocity to approach the relevant stream velocity. The influence of the parameters Gr, Gc, *M*, *K*, Sc, Sr, Du, Ec, k_r and Bn on velocity, temperature, concentration profiles and skin-friction, rate of heat transfer, rate of mass transfer coefficients can be analyzed from Figs 2, 3, 4, 5, 6, 7, 8, 9, 10, 11, 12, 13, 14, 15, 16, 17, 18, 19, 20, 21, 22 and 23.

Figures 2 and 3 present the effect of the thermal Grashof number Gr and solutal Grashof number Gc on the velocity profile of the flow field. It is observed from the velocity profiles that the effect of Gr is to enhance the velocity of the flow field at all the points since buoyancy force acts like a favorable pressure gradient which accelerates the fluid within the boundary layer. Similar effects are observed by increasing the solutal Grashof number Gc which also helps in accelerating the velocity of the flow field with a considerable reduction in the solutal boundary layer thickness. The effect of the magnetic field on velocity profiles in the boundary layer is depicted in Fig.4. From this figure it is seen that the velocity starts from a minimum value of zero at the surface and increases till it attains the peak value and then starts decreasing until it reaches the minimum value at the end of the boundary layer for all the values of magnetic field parameter (Hartmann number). It is interesting to note that the effect of the magnetic field decreases the value of the velocity profile throughout the boundary layer. The effect of the magnetic field is more prominent at the point of peak value, i.e., the peak value drastically decreases with increases in the value of the magnetic field, because the presence of magnetic field in an electrically conducting fluid introduces a force called the Lorentz force, which acts against the flow if the magnetic field is applied in the normal direction, as in the present problem. This type of resisting force slows down the fluid velocity as shown in Fig.4. Figure 5 shows the effects of the permeability of the porous medium parameter *K* on the velocity distribution. As shown, the velocity is increasing with the increasing dimensionless porous medium parameter. The effect of the dimensionless porous medium parameter *K* becomes smaller as *K* increases. Physically, this result can be achieved when the holes of the porous medium are very large so that the resistance of the medium may be neglected.

Figure 6 describes the effect of the Schmidt number Sc on the velocity profiles of the flow field which reveals that the velocity profile decreases with an increase in the value of the Schmidt number, i.e., the presence of heavier diffusing species has a retarding effect on the velocity of the flow field. The effect of the Schmidt number Sc on concentration profiles is as shown in Fig.7. It is observed from this figure that the effect of the Schmidt number Sc is to decrease the concentration distribution for lower values of Sc in the solutal boundary layer. It can be expected that the mass transfer rate increases as Sc increases, for all other parameters fixed, that is an increase in the Schmidt number Sc decreases the concentration boundary layer thickness which is associated with the reduction in the concentration profiles. Physically, the increase of Sc means a decrease of molecular diffusion *D*. Hence, the concentration of the species is higher for small values of Sc and lower for larger values of Sc. The effect of the Soret number Sr on the velocity profiles is shown in Fig.8. From the definition, the Soret number is the ratio of temperature difference to the concentration. Hence, a bigger Soret number stands for a larger temperature difference and precipitous gradient. From this figure it is observed that the velocity profiles increase with increasing the values of the Soret number Sr. Thus the fluid velocity rises due to a greater thermal diffusion factor. Figure 9 depicts the variation of concentration profiles for various values of Sr. We notice that there is a relative rise in the concentration profiles near the wall for the case when Sr = *10.0.* Higher values of Sr give rise to the formation of a peak near the wall. Further it is observed that the concentration distribution increases with increasing the Soret number Sr more effectively near the surface of the vertical plate.

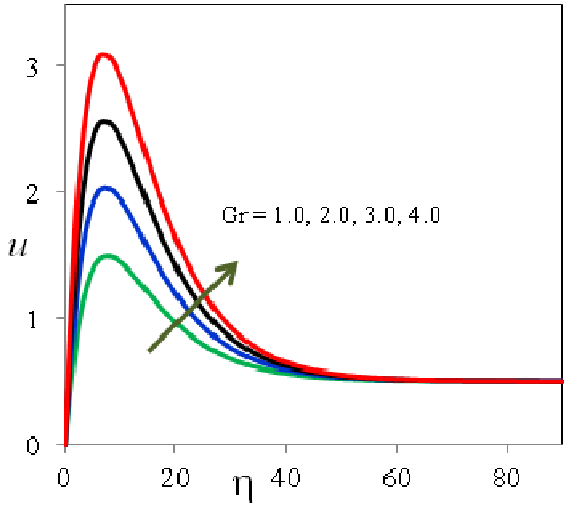

Fig.2. Velocity profiles for different values of Gr.

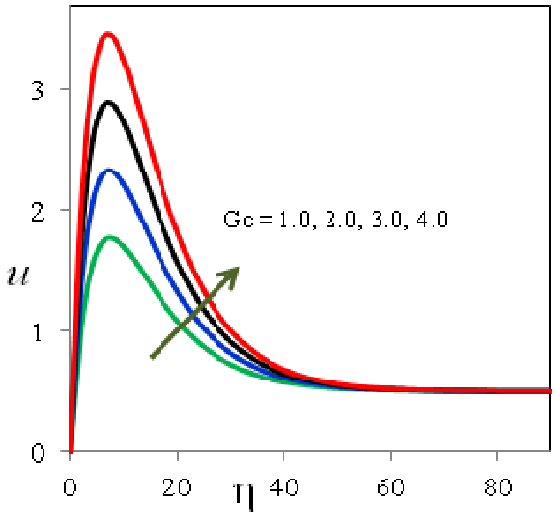

Fig.3. Velocity profiles for different values of Gc.

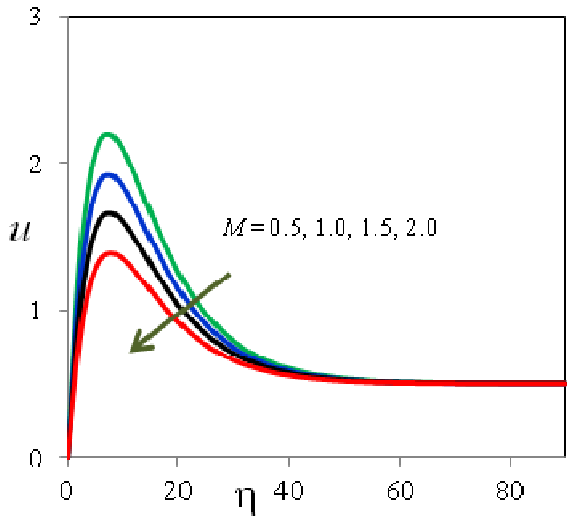

Fig.4. Velocity profiles for different values of *M*.

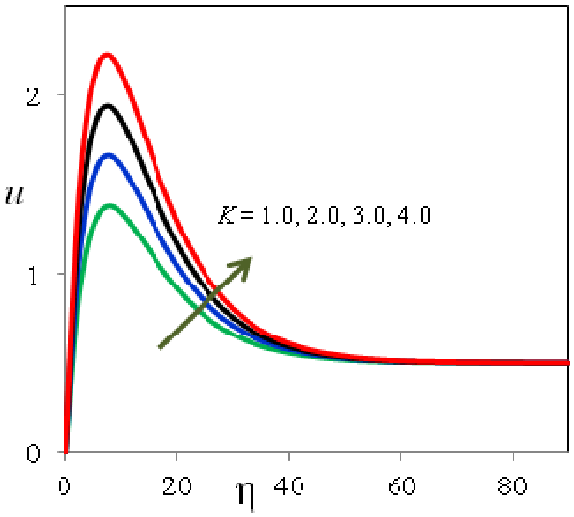

Fig.5. Velocity profiles for different values of *K*.

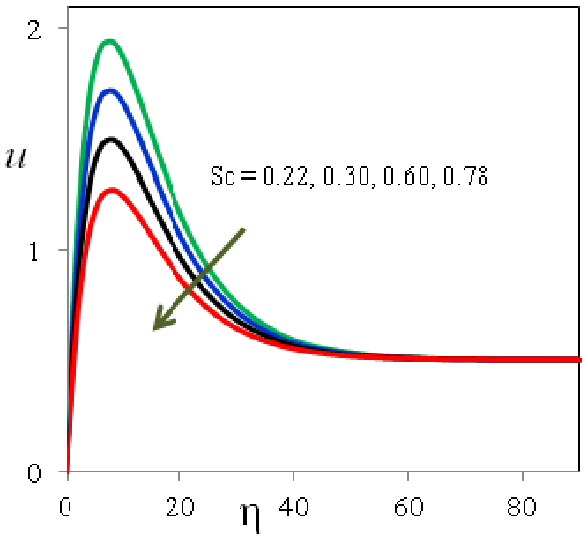

Fig.6. Velocity profiles for different values of Sc.

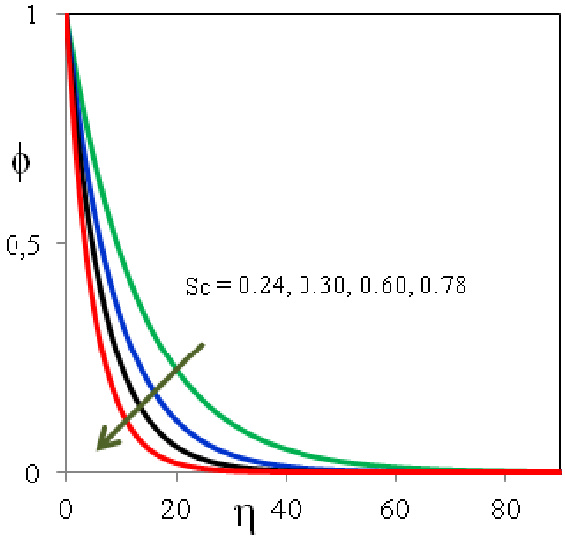

Fig.7. Concentration profiles for different values of Sc.

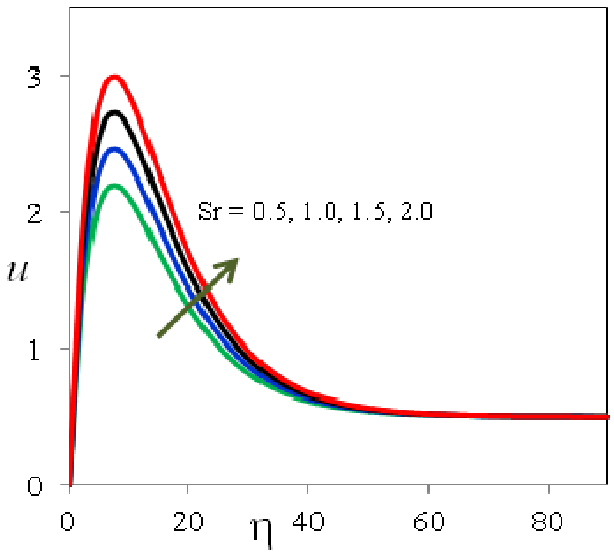

Fig.8. Velocity profiles for different values of Sr.

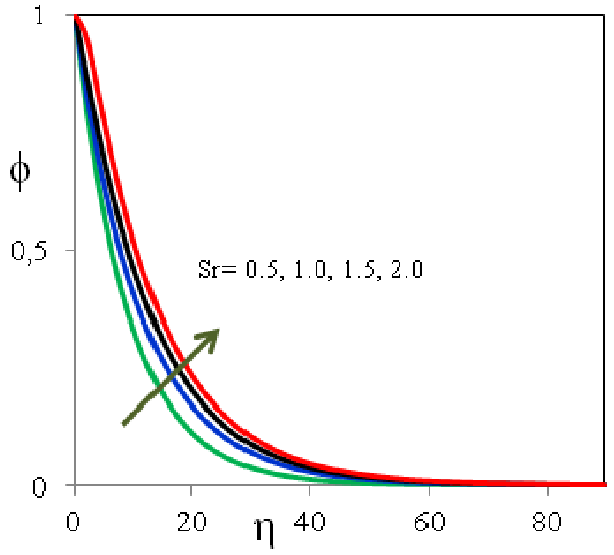

Fig.9. Concentration profiles for different values of Sr.

The velocity and temperature profiles with collective variation in Dufour number Du are plotted in Figs 10 and 11, respectively. Dufour number simulates the effect of concentration gradients on thermal energy flux in the flow domain. It is found that an increase in the Dufour number causes a rise in the velocity and temperature throughout the boundary layer. For, the temperature profiles decay smoothly from the plate to the free stream value. However for, a distinct velocity overshoot exists near the plate, and thereafter the profile falls to zero at the edge of the boundary layer. The effect of the viscous dissipation parameter i.e., the Eckert number Ec on the velocity and temperature are shown in Figs 12 and 13, respectively. The Eckert number Ec expresses the relationship between the kinetic energy in the flow and the enthalpy. It embodies the conversion of kinetic energy into internal energy by work done against the viscous fluid stresses. Greater viscous dissipative heat causes a rise in the temperature, as well as the velocity and cross flow velocity. This behaviour is evident from Figs 12 and 13. Figure 14 depicts the effect of chemical reaction parameter k_r on velocity profiles. It is observed that the effect of chemical reaction is to decrease the fluid velocity near the plate with decrease in the peak value.

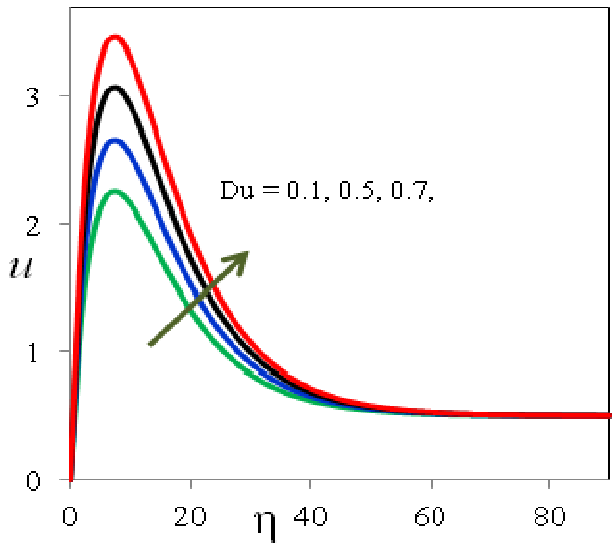

Fig.10. Velocity profiles for different values of Du.

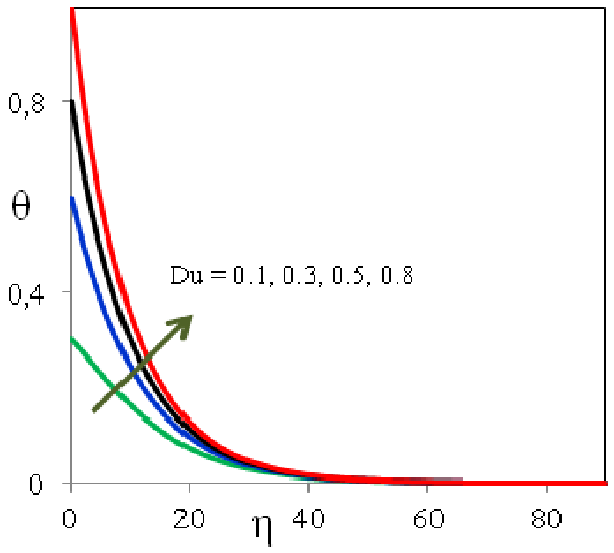

Fig.11. Temperature profiles for different values of Du.

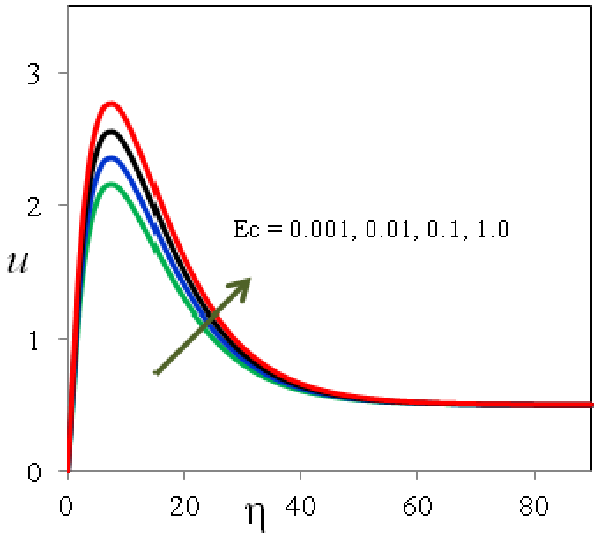

Fig.12. Velocity profiles for different values of Ec.

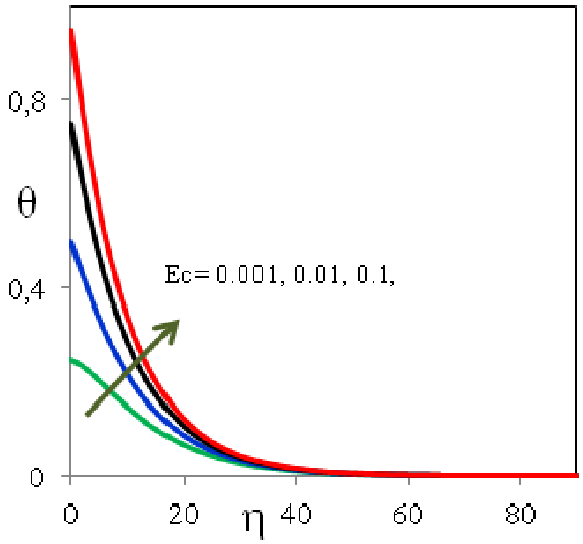

Fig.13. Temperature profiles for different values of Ec.

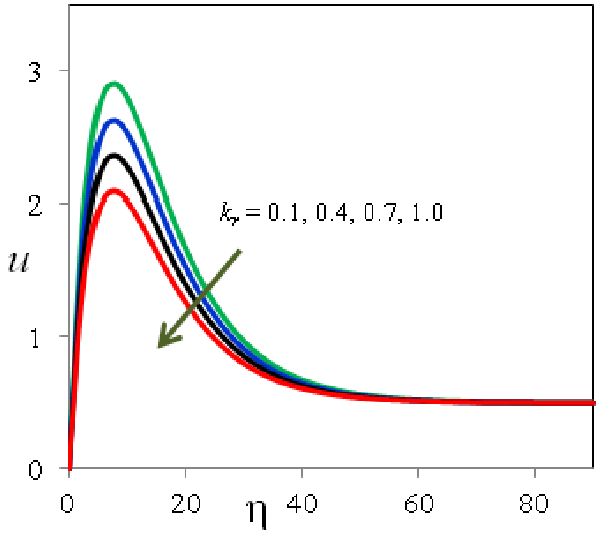

Fig.14. Velocity profiles for different values of k_r.

The effect the reaction rate parameter k_r on the species concentration profiles for generative chemical reaction is shown in Fig.15. It is noticed from the graph that there is a marked effect of increasing the value of the chemical reaction rate parameter k_r on concentration distribution in the boundary layer. It is clearly observed from this figure that the concentration of species which is greater than 1 at the start of the boundary layer decreases slowly till it attains the minimum value of zero at the end of the boundary layer and this trend is seen for all the values of the reaction rate parameter. Further, it is observed that increasing the value of the chemical reaction decreases the concentration of species in the boundary layer, this is due to the fact that a destructive chemical reaction reduces the solutal boundary layer thickness and increases the mass transfer. Figure 16 shows the velocity profiles with or without the Biot number. Here, we emphasize that the Biot number (Bn) is the ratio of the internal thermal resistance of the plate to the boundary layer thermal resistance. It is interesting to note that without the Biot number (i.e., Bn $= 0$, the left side of the plate with the hot fluid is totally insulated and no convective heat transfer to the cold fluid on the right side takes place) the peak velocity is low. As the convection Biot number increases, the plate thermal resistance reduces. Consequently, the peak velocity and the velocities in the neighbourhood of the peak increase significantly. This effect is triggered by stronger buoyancy forces induced as a result of the increase in the strength of the convective process at the plate. The effect of the Biot number (Bn) on temperature profiles is as shown in

Fig.17. It is interesting to note that the fluid temperature on the right side of the plate increases with an increase in the Biot number, since as Bn increases, the thermal resistance of the plate decreases and the convective heat transfer to the fluid on the right side of the plate increases. The effect of the Soret number on the skin-friction and rate of mass transfer coefficients is as shown in Figs 18 and 19, respectively. It is seen that an increase in the Soret number causes an enhancement in the skin-friction and the rate of mass transfer coefficients at all points. The influence of the Dufour number over the skin-friction and rate of heat transfer coefficients are elucidated with the help of Figs 20 and 21. It is clear that the skin-friction and rate of heat transfer coefficients are rising with an increase of Dufour number. The effect of the Biot number on the skin-friction and rate of mass transfer coefficients is as shown in Figs 22 and 23, respectively. It is seen that the growth of the Biot number causes an enhancement in the skin-friction and rate of mass transfer coefficients at all points. The comparison of the skin-friction and rate of heat transfer coefficients for dissimilar values of the Dufour number (Du) in the absence of the Biot number is shown in Fig.24. From this Fig.24, we noticed that the curves for the skin-friction and rate of heat transfer coefficients are close to each other.

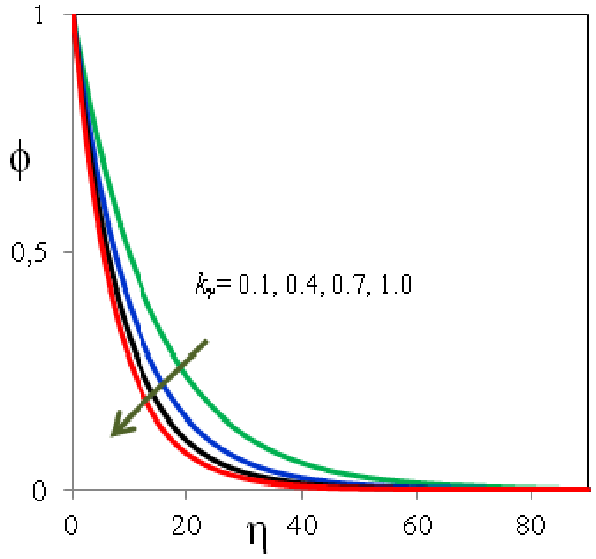

Fig.15. Concentration profiles for different values of k_r.

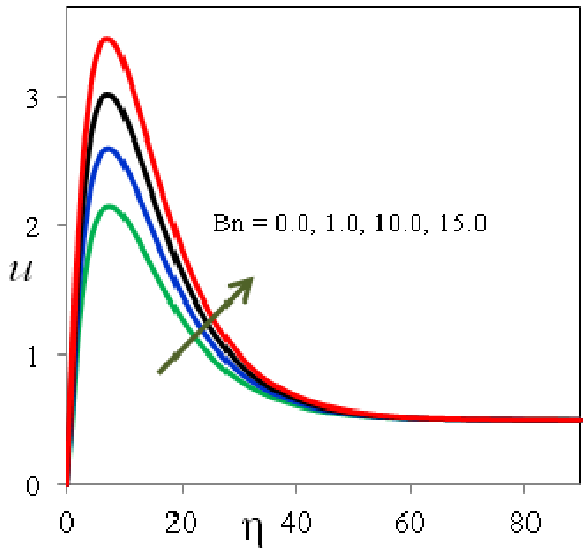

Fig.16. Velocity profiles for different values of Bn.

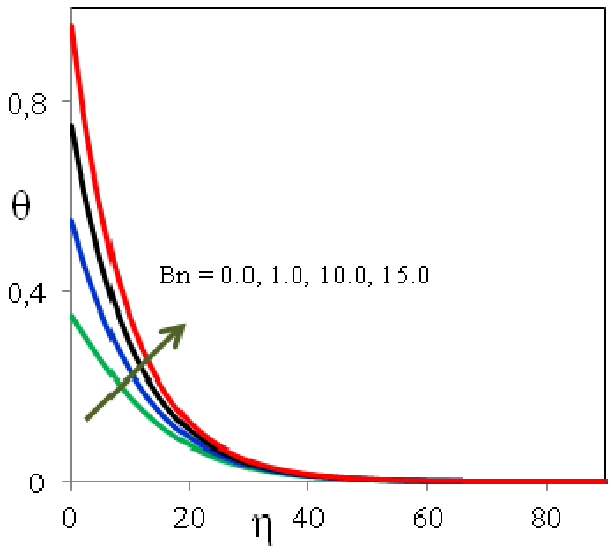

Fig.17. Temperature profiles for different values of Bn.

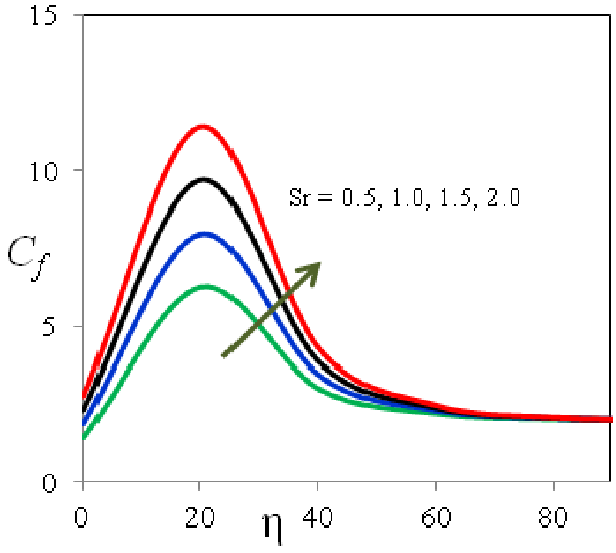

Fig.18. Skin-friction coefficient for different values of Sr.

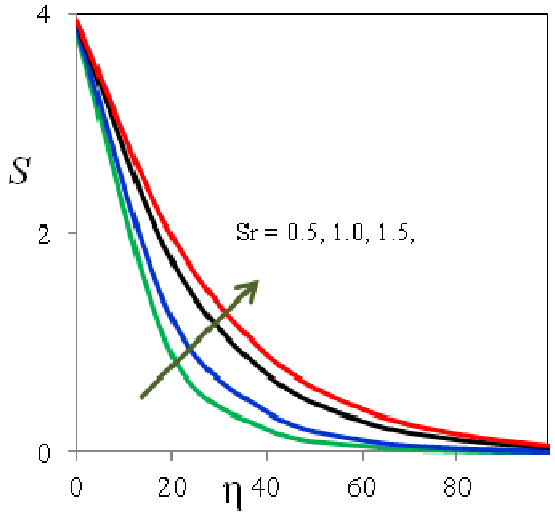

Fig.19. Rate of mass transfer coefficient for different values of Sr.

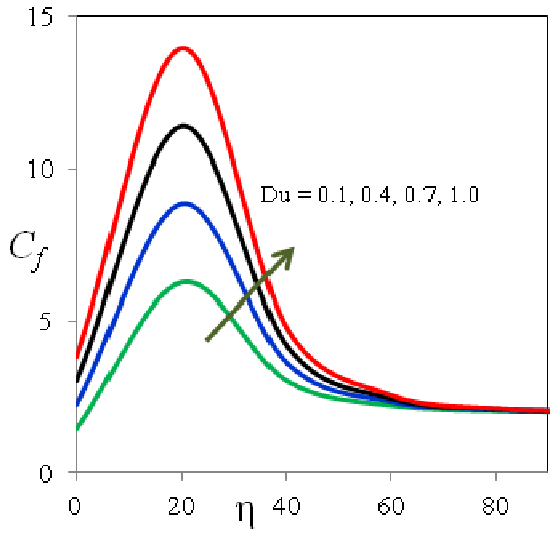

Fig.20. Skin-friction coefficient for different values of Du.

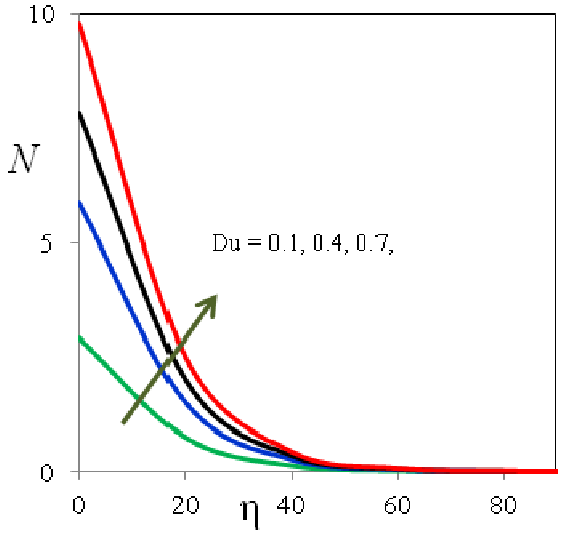

Fig.21. Rate of heat transfer coefficient for different values of Du.

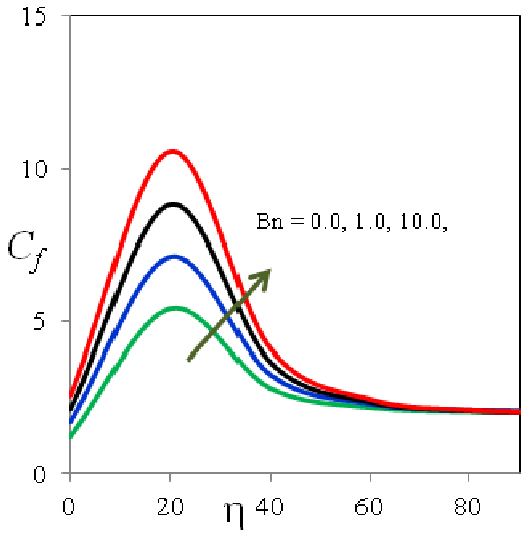

Fig.22. Skin-friction coefficient for different values of Bn.

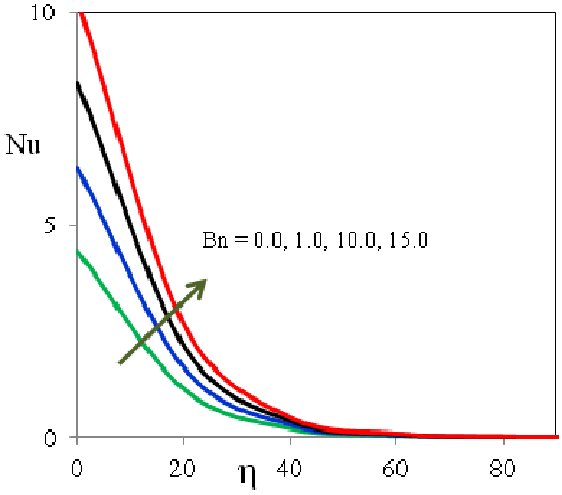

Fig.23. Rate of heat transfer coefficient for different values of Bn.

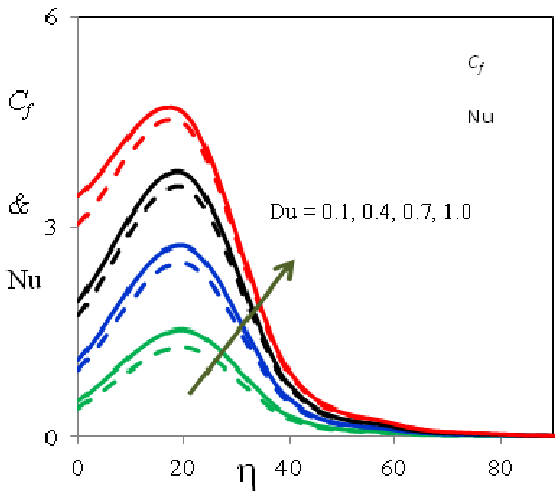

Fig.24. Comparison of skin-friction and rate of heat mass transfer coefficients for different values of Du.

4.1. Local skin-friction $\left(u'(0)\right)$

The numerical values of the local skin-friction are presented in Tab.2 for different values of the magnetic field, permeability of the porous medium, viscous dissipation, chemical reaction parameter, Soret, Dufour and Biot numbers. It is observed from this table that:

- the skin-friction increases from *1.891555124* to *2.526743816* with increasing the value of *M* from *0.1* to 10.0, while a reverse effect is found for k_r (skin-friction decreases from *1.891555124* to *1.886928855* with increasing the value of k_r from *0.1* to *2.0*),
- the increase in viscous dissipation (Ec) by a factor of 2 changes the local skin friction value from *1.907091911* to *1.920915361*,
- the skin-friction decreases as Sr decreases from *2.0* to *1.0*; thereafter however it increases with a subsequent lower in Sr from *1.0* through to the least value of *0.0*,
- the permeability of the porous medium (*K*) has a towering impact on skin-friction. When the permeability of the porous medium is decreased by a factor of 10, the skin-friction decreases from *1.891555124* to *0.759132115*, while a reverse effect is found for Du (skin-friction increases from *1.891555124* to *2.140619924* with increasing the value of Du from *0.0* to *2.0*),
- finally, the skin-friction increases Bn with the value of very significantly as the Bn increases from *0.1* to *10*.

4.2. Local rate of heat transfer $\left(-\theta'(0)\right)$

The mathematical values of the local rate of heat transfer are presented in Tab.2 for different values of the magnetic field, permeability of the porous medium, viscous dissipation, chemical reaction parameter, Soret, Dufour and Biot numbers. It is observed from this table that:

- the potency of the magnetic field (*M*) has a little impact on the local rate of heat transfer. For example, when the magnetic field is increased by a factor of 1, the plate temperature increases from *0.083172669* to *0.084068831*,
- the rate of heat transfer increases from *0.044871116* to *0.050865522* with an increase in the Eckert number (Ec) from *1.0* to *2.0*, while a reverse effect is found for k_r (rate of heat transfer decreases from *0.083620068* to *0.083615016* with increasing the value of k_r from *1.0* to *2.0*),
- as the Dufour number values increase from *1.0* to *2.0*, then the rate of heat transfer values increase from *0.153916278* to *0.210945624*, whereas an opposite effect is found for *K*,
- the effectiveness of the Soret number (Sr) (increases from *1.0* to *2.0*) has a minimum impact on rate of heat transfer (increases from *0.000532168* to *0.000638197*),
- finally, the rate of heat transfer increases as Bn increases very notably as the Bn increases from *0.1* to *10*.

4.3. Local rate of mass transfer $\left(-\varphi'(0)\right)$

The results of the local rate of mass transfer are presented in Tab.2 for different values of the magnetic field, permeability of the porous medium, viscous dissipation, chemical reaction parameter, Soret, Dufour and Biot numbers. It is observed from this table that:

- the effect of the Soret number is seen more prominently for the rate of mass transfer, i.e., there is a sharp increase in the value of the rate of mass transfer,
- the rate of mass transfer increases from *0.459012311* to *1.539295169* with an increase in the chemical reaction parameter k_r from *0.1* to *2.0*,
- there are no effects of *M*, *K* and Ec on the rate of mass transfer,

- the increase in the Dufour number (Du) by a factor of 2 changes the skin friction from a value of *10.459206478* to *0.460921378*,
- finally, the rate of mass transfer increases with the value of Du very significantly as the Du increases from *0.1* to *2.0.*

5. Conclusions

We have examined theoretically the effects of thermal diffusion and diffusion thermo on a magnetohydrodynamic mixed convective flow past a vertical plate embedded in a porous medium with chemical reaction and convective boundary condition. The computed values obtained from the numerical solutions of velocity, temperature, concentration fields are presented graphically and the local skin friction coefficient, the local Nusselt number, and the local Sherwood number are presented in a tabular form. The governing partial differential equations were transformed into ordinary differential equations. These equations were solved numerically by using the element free Galerkin algorithm. From the present investigation, the following conclusions are drawn:

1. the numerical results designate that the velocity increases with the increase in the Grashof number, Eckert number, permeability parameter, while it decreases as the magnetic field parameter and Schmidt number increases,
2. Dufour effects deeply influence the temperature profiles in the thermal boundary layer, i.e., temperature profiles increase with the increase in the Dufour number,
3. Soret effects are to enhance the concentration distribution with the formation of concentration peaks for superior values of the Soret parameter in the concentration boundary layer.
4. the velocity as well as concentration reduces with an increase in the chemical reaction parameter,
5. the numerical results obtained are compared with formerly reported cases available in the open literature and they are found to be in very good agreement,
6. physical significance and application of the Biot number with respect to boundary layer flow problems can be found in several engineering and industrial processes such as drying of material, transpiration cooling, etc.

The analysis has shown that the temperature and concentration fields are appreciably influenced by the Dufour and Soret effects. Thus we conclude that for some kind of mixture (i.e., H_2, air) with the light molecular weight, the Soret and Dufour effects play an important role and should be considered in future studies.

Nomenclature

B_o – transverse magnetic field $\left(A\,m^{-1}\right)$

Bn – Biot number

C^* – fluid concentration $\left(mol\ m^{-3}\right)$

C_f – skin-friction coefficient (pascal)

C_p – specific heat at constant pressure $\left(J\,Kg^{-1}K\right)$

C_s – concentration susceptibility $\left(m\ mole^{-1}\right)$

C_w^* – concentration at the wall $\left(mol\ m^{-3}\right)$

C_∞^* – concentration at free stream $\left(mol\ m^{-3}\right)$

D – solute mass diffusivity $\left(m^2\ s^{-1}\right)$

D_m – molecular diffusivity $\left(m^2\ s^{-1}\right)$
Du – Dufour number
Ec – Eckert number
Gc – Grashof number for mass transfer
Gr – Grashof number for heat transfer
g – acceleration due to gravity $\left(m\ s^{-2}\right)$
h_f – heat transfer coefficient
K – porosity (permeability) parameter $\left(m^2\right)$
K^* – dimensional porosity (permeability) parameter $\left(m^2\right)$
K_r^* – dimensional chemical reaction of first order with rate constant
k_r – chemical reaction parameter
k_T – mean absorption coefficient
M – Hartmann number
Nu – rate of heat transfer (or) Nusselt number
O – origin
Pr – Prandtl number
Re_x – Reynold's number
Sc – Schmidt number
Sh – rate of mass transfer (or) Sherwood number
Sr – Soret number
T^* – fluid temperature (K)
T_m – mean fluid temperature (K)
T_w^* – hot fluid temperature at the wall (K)
T_∞^* – fluid temperature at free stream (K)
U_p – free stream velocity $\left(m\ s^{-1}\right)$
U_p^* – dimensional free stream velocity $\left(m\ s^{-1}\right)$
u – dimensionless velocity $\left(m\ s^{-1}\right)$
u^* – velocity component in x^* - direction $\left(m\ s^{-1}\right)$
V_o – dimensional suction velocity $\left(m\ s^{-1}\right)$
x – dimensionless coordinate axis along the plate (m)
x^* – coordinate axis along the plate (m)
y – dimensionless coordinate axis normal to the plate (m)
y^* – coordinate axis normal to the plate (m)
β – coefficient of thermal expansion $\left(K^{-1}\right)$
β^{**} – coefficient of compositional expansion $\left(m^3\ Kg^{-1}\right)$
η – spatial coordinate
θ – dimensionless temperature (K)
κ – thermal conductivity $\left(W\ m^{-1}K^{-1}\right)$
ν – kinematic viscosity $\left(m^2\ s^{-1}\right)$

ρ – fluid density $\left(Kg\,m^{-3}\right)$

σ – electrical conductivity $\left(S\,m^{-1}\right)$

τ'_w – shear stress (pascal)

φ – dimensionless concentration $\left(mol\,m^{-3}\right)$

Superscript

$'$ – dimensionless properties

Subscripts

f – fluid
p – plate
w – wall condition
∞ – free stream condition

References

[1] Nield D.A. and Bejan A. (2013): *Convection in Porous Media*. – 4th Edition, New York: Springer.

[2] Rashidi M.M., Rostami B., Freidoonimehr N. and Abbasbandy S. (2014): *Free convective heat and mass transfer for MHD fluid flow over a permeable vertical stretching sheet in the presence of the radiation and buoyancy effects.* – Ain Shams Eng. J., vol.5, pp.901–912.

[3] Bég O.A., Uddin M.J., Rashidi M.M. and Kavyani N. (2014): *Double-diffusive radiative magnetic mixed convective slip flow with Biot and Richardson number effects*. – J. Eng. Thermophy., vol.23, pp.79–97.

[4] Freidoonimehr N., Rashidi M.M. and Mahmud S. (2015): *Unsteady MHD free convective flow past a permeable stretching vertical surface in a nano-fluid*. – Int. J. Thermal Sci., vol.87, pp.136–145.

[5] Dinarvand S., Doosthoseini A., Doosthoseini E. and Rashidi M.M. (2010): *Series solutions for unsteady laminar MHD flow near forward stagnation point of an impulsively rotating and translating sphere in presence of buoyancy forces*. – Nonlinear Anal. Real World Appl., vol.11, pp.1159–1169.

[6] Sheikholeslami M., Rashidi M.M. and Ganji D.D. (2015): *Numerical investigation of magnetic nanofluid forced convective heat transfer in existence of variable magnetic field using two phase model*. – J. Mol. Liq., vol.212, pp.117–126.

[7] Sheikholeslami M., Vajravelu K. and Rashidi M.M. (2016): *Forced convection heat transfer in a semi annulus under the influence of a variable magnetic field*. – Int. J. Heat Mass Transf., vol.92, pp.339–348.

[8] Sivaiah S. and Srinivasa Raju R. (2013): *Finite element solution of heat and mass transfer flow with Hall current heat source and viscous dissipation*. – Appl. Math. Mech., vol.34, pp.559–570.

[9] Garoosi F., Bagheri G. and Rashidi M.M. (2015): *Two phase simulation of natural convection and mixed convection of the nanofluid in a square cavity*. – Powder Technol., vol.275, pp.239–256.

[10] Makinde O.D. and Aziz A. (2010): *MHD mixed convection from a vertical plate embedded in a porous medium with a convective boundary condition*. – Int. J. Thermal Sci., vol.49, pp.1813–1820.

[11] Anand Rao J., Sivaiah S. and Srinivasa Raju R. (2012): *Chemical reaction effects on an unsteady MHD free convection fluid flow past a semi–infinite vertical plate embedded in a porous medium with heat absorption*. – J. Appl. Fluid Mech., vol.5, pp.63–70.

[12] Siva Reddy Sheri and Srinivasa Raju R. (2016): *Transient MHD free convective flow past an infinite vertical plate embedded in a porous medium with viscous dissipation*. – Meccanica, vol.51, No.5, pp.1057-1068.

[13] Ramana Murthy M.V., Srinivasa Raju R. and Anand Rao J. (2015): *Heat and mass transfer effects on MHD natural convective flow past an infinite vertical porous plate with thermal radiation and Hall current*. – Procedia Eng. J., vol.127, pp.1330–1337.

[14] Srinivasa Raju R., Mahesh Reddy B., Rashidi M.M. and Gorla R.S.R. (2016): *Application of finite element method to unsteady MHD free convection flow past a vertically inclined porous plate including thermal diffusion and diffusion thermo effects*. – J. Porous Media (In Press).

[15] Nejad M.M., Javaherdeh K. and Moslemi M. (2015): *MHD mixed convection flow of power law non-Newtonian fluids over an isothermal vertical wavy plate.* – J. Magn. Magn. Mater., vol.389, pp.66–72.

[16] Xiao-dong WANG., Guang-ya ZHU. and Lei WANG. (2015): *Exact analytical solutions for moving boundary problems of one-dimensional flow in semi-infinite porous media with consideration of threshold pressure gradient*. – J. Hydrodyn., Ser B, vol.27, pp.542–547.

[17] Vajravelu K., Prasad K.V. and Raju B.T. (2013): *Effects of variable fluid properties on the thin film flow of Ostwald-de Waele fluid over a stretching surface*. – J. Hydrodyn., Ser B, vol.25, pp.10–19.

[18] Saleem S. and Nadeem S. (2015): *Theoretical analysis of slip flow on a rotating cone with viscous dissipation effects*. – J. Hydrodyn. Ser B, vol.27, pp.616–623.

[19] Adesanya S.O. and Makinde O.D. (2015): *Thermodynamic analysis for a third grade fluid through a vertical channel with internal heat generation*. – J. Hydrodyn. Ser B 27, pp.264–272.

[20] Swati Mukhopadhyay and Vajravelu K. (2013): *Diffusion of chemically reactive species in Casson fluid flow over an unsteady permeable stretching surface*. – J. Hydrodyn. Ser B 25, pp.591–598

[21] Eckeret E.R.G. and Drake R.M. (1972): *Analysis of Heat and Mass Transfer*. – New York: McGraw Hill.

[22] Rashidi M.M., Hayat T., Erfani E., Mohimanian Pour S.A. and Hendi A.A. (2011): *Simultaneous effects of partial slip and thermal-diffusion and diffusion-thermo on steady MHD convective flow due to a rotating disk.* – Commun. Nonlinear Sci. Numer. Simul., vol.16, pp.4303–4317.

[23] Siva Reddy Sheri and Srinivasa Raju R. (2015): *Soret effect on unsteady MHD free convective flow past a semi-infinite vertical plate in the presence viscous dissipation*. – Int. J. Comput. Methods Eng. Sci. Mech., vol.16, pp.132–141.

[24] Raju R.S., Sudhakar K. and Rangamma M. (2013): *The effects of thermal radiation and Heat source on an unsteady MHD free convection flow past an infinite vertical plate with thermal diffusion and diffusion thermo*. – J. Inst. Eng. (India): Series C 94, pp.175–186.

[25] Anand Rao J. and Srinivasa Raju R. (2011): *The effects of Hall currents, Soret and Dufour on MHD flow and heat transfer along a porous flat plate with mass transfer*. – J. Energy Heat Mass Transfer, vol.33, pp.351–372.

[26] Srinivasacharya D., Mallikarjuna B. and Bhuvanavijaya R. (2015): *Soret and Dufour effects on mixed convection along a vertical wavy surface in a porous medium with variable properties*. – Ain Shams Eng. J., vol.6, pp.553–564.

[27] Mahdy A. and Ahmed S.E. (2015): *Thermosolutal Marangoni boundary layer magnetohydrodynamic flow with the Soret and Dufour effects past a vertical flat plate*. – Eng. Sci. Technol., vol.18, pp.24–31.

[28] Vedavathi N., Ramakrishna K. and Jayarami Reddy K. (2015): *Radiation and mass transfer effects on unsteady MHD convective flow past an infinite vertical plate with Dufour and Soret effects*. – Ain Shams Eng. J., vol.6, pp.363–371.

[29] Chao-Yin Hsiao, Wen-Jeng Chang, Ming-I Char and Bo-Chen Tai (2014): *Influence of thermophoretic particle deposition on MHD free convection flow of non-Newtonian fluids from a vertical plate embedded in porous media considering Soret and Dufour effects*. – Appl. Math. Comput., vol.244, pp.390–397.

[30] Dulal Pal and Sewli Chatterjee (2013): *Soret and Dufour effects on MHD convective heat and mass transfer of a power–law fluid over an inclined plate with variable thermal conductivity in a porous medium*. – Appl Math Comput., vol.219, pp.7556–7574.

[31] Dulal Pal and Hiranmoy Mondal (2013): *Influence of thermophoresis and Soret-Dufour on magnetohydrodynamic heat and mass transfer over a non-isothermal wedge with thermal radiation and Ohmic dissipation*. – J. Magn. Magn. Mater., vol.331, pp.250–255.

[32] Srinivasa Raju R., Jithender Reddy G., Anand Rao J., Rashidi M.M. and Gorla R.S.R. (2016): *Analytical and Numerical study of unsteady MHD free convection flow over an exponentially moving vertical plate with heat absorption*. – Int. J. Thermal Sci. (In Press).

[33] Ching-Yang Cheng (2012): *Soret and Dufour effects on free convection heat and mass transfer from an arbitrarily inclined plate in a porous medium with constant wall temperature and concentration*. – Int. Commun. Heat Mass Transf., vol.39, pp.72–77.

[34] Ching-Yang Cheng (2011): *Soret and Dufour effects on natural convection heat and mass transfer near a vertical wavy cone in a porous medium with constant wall temperature and concentration.* – Int. Commun. Heat Mass Transf. vol.38, pp.1056–1060.

[35] Dulal Pal and Sewli Chatterjee (2011): *Mixed convection magnetohydrodynamic heat and mass transfer past a stretching surface in a micropolar fluid–saturated porous medium under the influence of Ohmic heating, Soret and Dufour effects*. – Commun. Nonlinear Sci. Numer. Simul., vol.16, pp.1329–1346.

[36] Srinivasa Raju R., Jithender Reddy G., Anand Rao J., Rashidi M.M. and Gorla R.S.R. (2016): *Analytical and Numerical study of unsteady MHD free convection flow over an exponentially moving vertical plate with heat absorption*. – Int. J. Thermal Sci., vol.107, pp.303–315.

[37] Singh A., Singh I.V. and Prakash R. (2007): *Numerical analysis of fluid squeezed between two parallel plates by meshless method*. – Comput. Fluids, vol.36, pp.1460–1480.

[38] Singh I.V. (2004): *A numerical solution of composite heat transfer problems using meshless method*. – Int. J. Heat Mass Transf., vol.47, pp.2123–2138.

[39] Zhu T. and Atluri S.N. (1998): *A modified collocation method and a penalty formulation for enforcing the essential boundary conditions in the element free Galerkin method*. – Comput. Mech., vol.21, pp.211–222.

[40] Smith G.D. (1985): *Numerical Solutions of Partial Differential Equations–Finite Difference Methods*. – 3rd Edition, New York: Oxford University Press.

Received: May 4, 2016

Revised: June 6, 2017